

Citation for published version:
Moss, AC, Wright, CJ & Mitchell, NJ 2016, 'Does the Madden-Julian Oscillation modulate stratospheric gravity waves?', Geophysical Research Letters, pp. 3973-3981. https://doi.org/10.1002/2016GL068498

DOI: 10.1002/2016GL068498

Publication date: 2016

Document Version Publisher's PDF, also known as Version of record

Link to publication

Publisher Rights CC BY

University of Bath

Alternative formats

If you require this document in an alternative format, please contact: openaccess@bath.ac.uk

General rights

Copyright and moral rights for the publications made accessible in the public portal are retained by the authors and/or other copyright owners and it is a condition of accessing publications that users recognise and abide by the legal requirements associated with these rights.

If you believe that this document breaches copyright please contact us providing details, and we will remove access to the work immediately and investigate your claim.

Download date: 12. Mar. 2023



Geophysical Research Letters

RESEARCH LETTER

10.1002/2016GL068498

Key Points:

- MJO signature observed in stratospheric gravity waves
- Strong anticorrelation between gravity wave energy and eastward zonal wind anomalies
- Evidence that the MJO modulates stratospheric gravity wave activity through wave filtering

Supporting Information:

Supporting Information S1

Correspondence to:

A. C. Moss, andrew.moss@bath.edu

Citation:

Moss, A. C., C. J. Wright, and N. J. Mitchell (2016), Does the Madden-Julian Oscillation modulate stratospheric gravity waves?, *Geophys. Res. Lett.*, 43, doi:10.1002/2016GL068498.

Received 2 MAR 2016 Accepted 30 MAR 2016 Accepted article online 4 APR 2016

Does the Madden-Julian Oscillation modulate stratospheric gravity waves?

Andrew C. Moss¹, Corwin J. Wright¹, and Nicholas J. Mitchell¹

¹Centre for Space, Atmospheric and Oceanic Science, University of Bath, Bath, UK

Abstract The circulation of the stratosphere is strongly influenced by the fluxes of gravity waves propagating from tropospheric sources. In the tropics, these gravity waves are primarily generated by convection. The Madden-Julian Oscillation (MJO) dominates the intraseasonal variability of this convection. However, the influence of the MJO on the variability of stratospheric gravity waves is largely unknown. Here we examine gravity wave potential energy at 26 km and the upper tropospheric zonal wind anomaly of the MJO at 200 hPa, sorted by the relative phase of the MJO using the Real Multivariate MJO indices. We show that a strong anticorrelation exists between gravity wave potential energy and the MJO eastward wind anomaly. We propose that this correlation is a result of the filtering of upward propagating waves by the MJO winds. The study provides the first observational evidence that the MJO contributes significantly to the global variability of stratospheric gravity waves in the tropics.

1. Introduction

Gravity waves play a very important role in the dynamics of the stratosphere. The waves can propagate upward from their sources in the troposphere upward to greater heights, resulting in a vertical flux of energy and horizontal momentum. When the waves dissipate, this energy and momentum are transferred to the mean flow.

Gravity waves can be generated by a variety of sources, including winds blowing over mountains and the adjustment of jet streams. In the tropics, deep tropospheric convection associated with cumulus clouds is the main source of gravity waves [e.g., Alexander et al., 2008; Wright and Gille, 2011]. Such tropical waves drive important features of the tropical stratospheric circulation, including the quasi-biennial oscillation (QBO) and semiannual oscillation (SAO) [e.g., Hamilton et al., 2004]. Measurements of the fluxes and variability of gravity waves and how these are related to their sources are thus essential in efforts to understand the dynamics of the stratosphere and in efforts to develop numerical weather prediction and climate models [e.g., Fritts and Alexander, 2003; Alexander et al., 2010].

Tropical cumulus convection itself varies significantly on intraseasonal time scales (i.e., time scales of $\sim 10-100$ days). The largest component of this variability is the Madden-Julian oscillation (MJO) [Madden and Julian, 1972], which is the most prominent intraseasonal oscillation (ISO). The MJO is a large-scale repeating pattern of coupled circulation and deep convection that originates in the Indian Ocean and then propagates eastward to the western/central Pacific. It has a period of $\sim 30-90$ days and typically travels at $\sim 5~{\rm m~s^{-1}}$ [e.g., Zhang, 2005]. While the convection of the MJO is largely confined to the Eastern Hemisphere, its dynamical influence is apparent on a global scale [e.g., Salby et al., 1994]. The MJO is known to be closely associated with convectively coupled Rossby and Kelvin waves [e.g., Matthews, 2000; Sperber, 2003; Khouider et al., 2011]. Anomalies in tropospheric zonal wind are observed toward the MJO center close to the surface (850 hPa) and away from the MJO center in the upper troposphere (200 hPa), as presented schematically in Figure 1. In light of the known role of the MJO in modulating tropical convection, we can thus ask the question does the MJO act to modulate the variability of stratospheric gravity waves?

To date, there have only been a very limited number of attempts to determine the influence of the MJO on the variability of gravity waves in the tropical stratosphere. In particular, *Horinouchi* [2008] used a cloud-resolving model to investigate convectively generated gravity waves and their propagation into the stratosphere. He found that upward propagation of gravity waves was significantly increased during the inactive phase of the MJO (when there is actually reduced convection). This apparently counter-intuitive result is a consequence of

©2016. The Authors.

This is an open access article under the terms of the Creative Commons
Attribution License, which permits use, distribution and reproduction in any medium, provided the original work is properly cited.

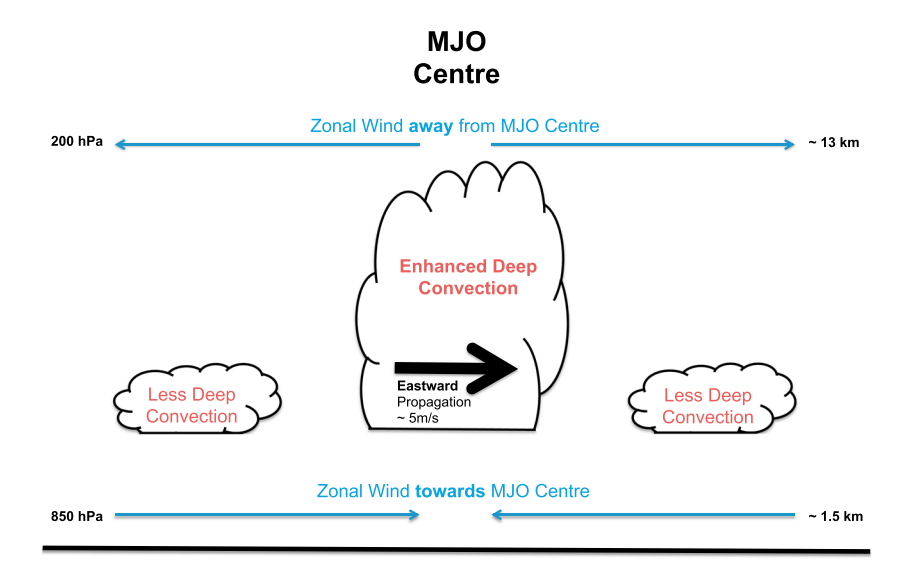


Figure 1. Schematic diagram showing some characteristics of the Madden-Julian Oscillation. Adapted from

the modeled gravity waves generated in the inactive phase of the MJO having (i) higher phase speeds and (ii) longer vertical wavelengths than those gravity waves generated in the active phase. This arises from the greater convective cloud rain-top heights associated with the inactive phase of the MJO [e.g., Morita et al., 2006]. These gravity waves of higher phase speed and longer vertical wavelength are better able to propagate into the stratosphere where they account for the increased gravity wave fluxes.

In contrast, Karoly et al. [1996] considered radiosonde data from Santa Cruz (10°S, 165°E) in the South Pacific recorded during the 4 month Tropical Ocean Global Atmosphere-Coupled Ocean-Atmosphere Response Experiment campaign of 1992 – 1993 when the MJO had significant amplitude. They reported significant correlations between gravity wave activity in the lower stratosphere (17-24 km) and proxies for convective activity including outgoing long-wave radiation (OLR), thus suggesting a positive correlation between the MJO convection and gravity wave activity in the lower stratosphere.

There is some evidence that ISOs in tropospheric convection, including the MJO, modulate the fluxes of gravity waves and/or nonmigrating tides in the tropical mesosphere and lower thermosphere (MLT). Eckermann et al. [1997] reported that gravity wave variances and MLT winds both display fluctuations at ISO periodicities. They proposed that ISOs, including the MJO, may be modulating the generation of gravity waves and nonmigrating tides that then subsequently propagate through the stratosphere to the MLT where their modulated momentum fluxes drive fluctuations in the winds at ISO periods when the gravity waves and/or tides dissipate. This suggestion has received support from other observations of fluctuations in MLT region winds at ISO and MJO periodicities [e.g., Davis et al., 2012; Rao et al., 2009]. However, other studies have argued that nonmigrating tides drive the MLT region ISOs, and so the role of modulated gravity wave fluxes remains unclear [e.g., Isoda et al., 2004].

We thus see that there is great uncertainty regarding the magnitude and phasing of any connection between the MJO and stratospheric gravity waves. However, establishing the nature of any such modulation is important in attempts to understand the coupling of the tropical troposphere and stratosphere. These uncertainties highlight the need for studies to determine the magnitude and relative phasing of any MJO influence on the field of convectively generated gravity waves.

Here we present observations of gravity wave potential energies (GWPE) made in the tropical lower stratosphere from Constellation Observing System for Meteorology, Ionosphere, and Climate (COSMIC) radio occultation satellite observations. GWPE at 26 km and zonal wind anomalies at 200 hPa pressure level are examined to investigate their intraseasonal variability. The fundamental novelty of our analysis is to sort our observations of stratospheric gravity waves by the phase of the MJO defined by the Real Multivariate MJO (RMM) indices [Wheeler and Hendon, 2004]. This is the first time this analysis has been applied to stratospheric gravity waves. Finally, we propose and provide evidence for a mechanism by which this stratospheric gravity wave variability is caused by the MJO.



2. Data and Analysis

2.1. COSMIC GPS-RO Gravity Wave Observations

The COSMIC mission was launched in April 2006 and consists of six low-Earth orbiting satellites that track GPS satellites as they rise or set over the horizon. The radio signal received by these satellites is influenced by the atmospheric limb. Vertical profiles of temperature and pressure can be computed from the phase delay of the signal [Liou et al., 2007]. COSMIC data have been extensively used for a number of gravity wave studies [e.g., Alexander et al., 2008, 2009; Wang and Alexander, 2010; Wright et al., 2011; McDonald, 2012; Faber et al., 2013; Hindley et al., 2015].

Here we use COSMIC level-2 dry atmospheric temperature data from September 2006 to December 2012. GPS radio occultation (GPS-RO) measurements have sub-Kelvin temperature precision [Tsuda et al., 2011], horizontal resolution in the stratosphere of ~270 km [Kursinski et al., 1997; Hindley et al., 2015], and features with vertical scales greater than 2 km can be distinguished from noise [Marquardt and Healy, 2005; Tsuda et al., 2011]. Thus, we interpolate all COSMIC profiles to 2 km resolution prior to analysis and as a result will only observe gravity waves with vertical wavelengths greater than 4 km. In addition, limb sounding instruments, such as COSMIC, are most sensitive to mid- and low-frequency gravity waves (i.e., inertia-gravity waves) that have short vertical and long horizontal wavelengths [e.g., Wright et al., 2015]. Hence, our results are only representative of this part of the wave spectrum.

For each day of data, the COSMIC temperature profiles are binned onto a 10° × 20° latitude-longitude grid, stepped in 1° × 1° increments. Zonal mean and planetary-scale features of zonal wave number 0-6, such as Kelvin waves, are calculated at each latitude and height. The resulting local background temperature profile, \bar{T} , is removed from each original temperature profile by interpolating to its latitude-longitude position to reveal the temperature perturbations due to gravity waves alone. We next apply an S Transform [Stockwell et al., 1996] to each temperature perturbation profile, T', to determine the largest resulting wave amplitude at each height. This amplitude is used to calculate the potential energy, E_p , [Tsuda et al., 2000] for each height using equation (1), where the acceleration due to gravity, g, is assumed to be constant and N is the Brunt-Väisälä frequency.

$$E_p = \frac{1}{2} \left(\frac{g}{N} \right)^2 \left(\frac{T'}{\bar{T}} \right)^2 \tag{1}$$

The GWPE for each day is then defined as the average E_p for each 10° \times 20° latitude-longitude cell at a height of 26 km. The time series of GWPE in each cell is then bandpassed with a 201-point Lanczos filter [Duchon, 1979] with half-power points at 20 and 100 day periods to reveal any intraseasonal variability in the data. This bandpassing method closely follows the methodology of the CLIVAR Madden-Julian Oscillation Working Group [2009], who presented a standardized method of identifying MJO signals in atmospheric data.

2.2. ECMWF Zonal Wind

European Centre for Medium Range Weather Forecasting (ECMWF) operational analysis data are used to calculate zonal wind anomalies at the 200 hPa pressure level. The data used are from the 1.125° resolution data set and are bandpassed for each grid point in the same way as GWPE to filter for intraseasonal variability.

2.3. RMM MJO Index

 $The \, Real-time \, Multivariate \, MJO \, (RMM) \, index \, of \, \textit{Wheeler and Hendon} \, [2004] \, defines \, the \, daily \, variation \, in \, ampli-like \, (and \, like \,$ tude and phase of the MJO for eight specific phases. The index is composed of a combination of equatorially averaged anomalies of OLR and zonal wind at 850 hPa and 200 hPa projected onto the leading pair of empirical orthogonal functions [Wheeler et al., 2009].

Here we use the MJO index to create composite maps for our data for each MJO phase. Data are only used in the composite average for each phase if they fall within that phase, and the amplitude of the RMM index exceeds 1 (i.e., a strong MJO is present). This analysis results in maps of 20-100 day bandpassed GWPE and 200 hPa zonal wind anomalies for each MJO phase. It thus provides an appropriate tool to investigate the connection between stratospheric gravity waves and the MJO. This 20 – 100 day period range is specifically chosen because it is that used to evaluate MJO simulations in the consistent framework of CLIVAR Madden-Julian Oscillation Working Group [2009]. We will refer to the 20 – 100 day period range as the "MJO period range" from here onward.

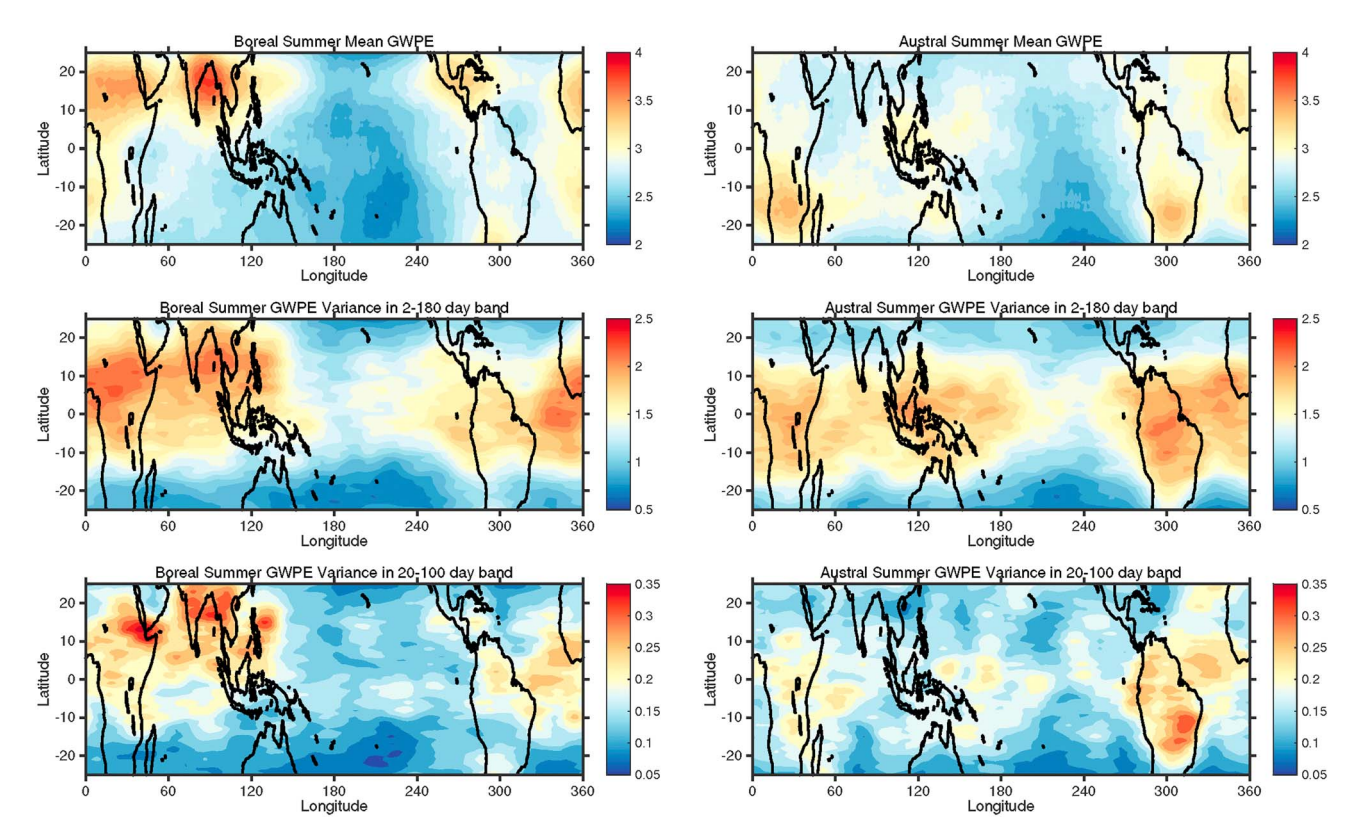


Figure 2. Composite mean plots of gravity wave potential energy (GWPE) for (left column) boreal summer (May to October) and (right column) austral summer (November to April). (top row) The mean GWPE for each season. (middle row) The variance of GWPE in the intraannual bandpass (2–180 day) for each season. (bottom row) The variance of GWPE in the intraseasonal bandpass (20–100 day) for each season. The units for Figure 2 (top row) of mean GWPE are in J kg $^{-1}$. For all other panels showing the variance of GWPE, the units are in J2 kg $^{-2}$.

3. Results

The geographical and seasonal variability of GWPE is presented in Figure 2. Figure 2 (left column, from top to bottom) shows mean GWPE, the variance of 2–180 day bandpassed GWPE, and the variance of MJO period range GWPE as composites averaged over boreal summer months (May to October). Mean GWPE is enhanced over Africa, the Bay of Bengal, and Central America. The variances of the 2–180 day and MJO period range GWPE are more widely distributed around the tropics.

Figure 2 (right column) shows the same analysis but averaged over the austral summer months (November to April). There are enhanced regions of mean GWPE over southern Africa, Indonesia, and South America, and the variance of bandpassed GWPE is more uniformly distributed. Lower energies are observed in austral summer compared to boreal summer, and the largest values tend to be in the summer hemisphere, as is especially evident in the panels showing mean GWPE. Comparison of the intraannual and intraseasonal gravity wave variances shows that there is a significant proportion of variability associated with ISOs.

The RMM indices of Wheeler and Hendon [2004] provide a method of identifying whether the ISOs in observational data exhibit a correlation with the MJO. Figure 3 presents mean composites of MJO period range GWPE (filled contours) and MJO period range zonal wind anomalies at 200 hPa (colored lines) for each phase of the RMM indices where a strong MJO is present (where the amplitude of the RMM index is greater than 1). Purple solid lines indicate regions of increased eastward zonal wind, and green dash-dotted lines indicate regions of increased westward zonal wind. The number of days noted on the right axis of each phase composite represent the number of days used to calculate that particular composite mean.

A clear eastward movement of both GWPE and zonal wind anomalies around the entire tropical belt is observed as the phase of the MJO progresses. The amplitude of the GWPE anomalies are $\sim 0.15 \, \text{J kg}^{-1}$.

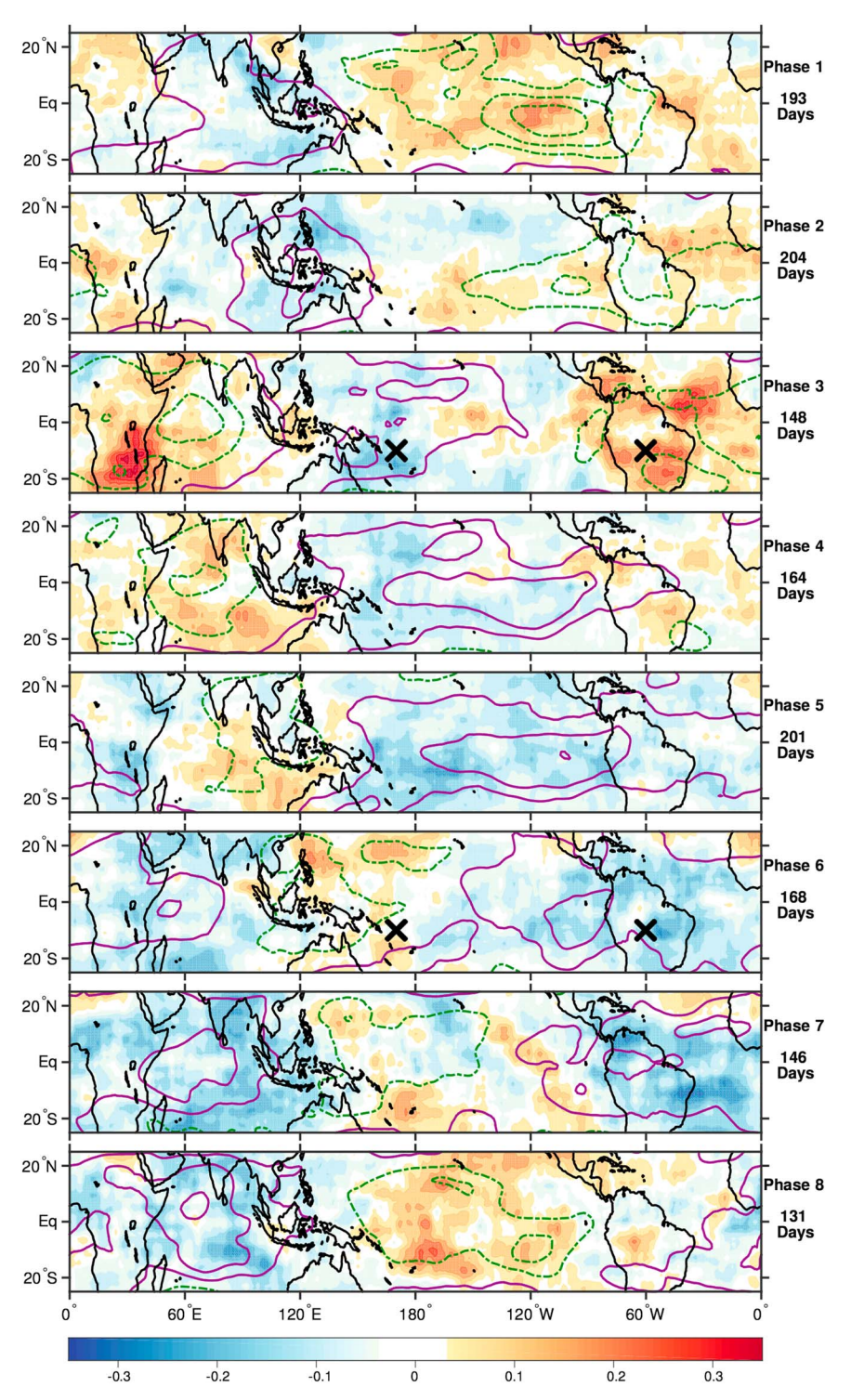


Figure 3. Composite plots of 20-100 day bandpassed zonal wind anomalies and 20-100 day bandpassed GWPE averaged over all days for each phase of the RMM MJO Index where the amplitude exceeded 1 (number of days indicated on the right axis of each panel). Zonal wind data are shown as purple solid (+ve) and green dash-dotted (-ve) contours in intervals of ± 2 m s⁻¹ from 1 m s⁻¹. The black crosses on the panels for phases 3 and 6 indicate two locations where wave filtering was compared (see Figure 4). Units of GWPE are in J kg^{-1} .

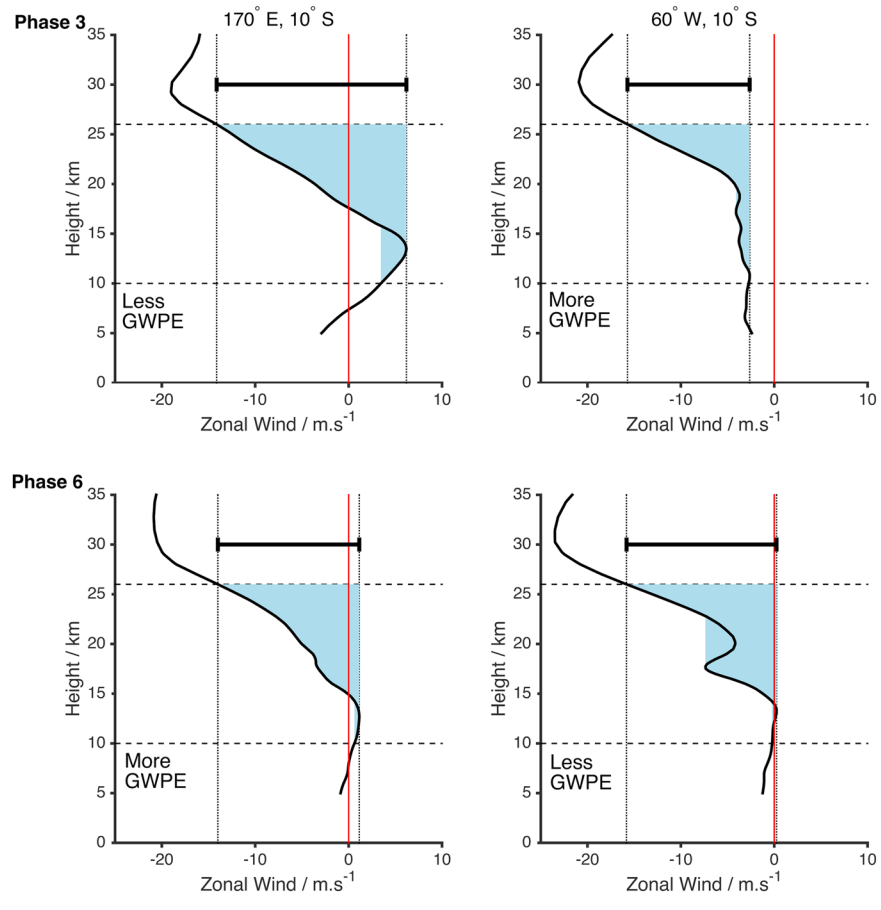


Figure 4. Nonbandpassed ECMWF zonal wind profiles for the two locations indicated by crosses in Figure 3 for MJO phase 3 and phase 6. The dark blue shaded region on each plot shows the range of winds encountered as waves ascend between 10 km and 26 km. The total range of winds encountered between these heights is illustrated by the black bar at the top of each panel.

This amounts to approximately 5-10% of the total GWPE evident in Figure 2. This is in contrast to the convective signature of the MJO (see supporting information Figure S1), which is mostly confined to the Eastern Hemisphere.

There appears to be a very close correlation between GWPE and these zonal wind anomalies. Specifically, stronger eastward winds appear to occur at the same time as a depression in GWPE and stronger westward winds when GWPE is increased. This suggests that the dynamic response (i.e., the zonal wind anomalies at 200 hPa—see Figure 1) of the MJO has a stronger influence on the stratospheric GWPE than the source variability evidenced by OLR.

To quantify the relationship between the MJO characteristics and GWPE, we correlate the MJO period range GWPE and the MJO period range 200 hPa zonal winds. A strong anticorrelation of \sim -0.8 is observed between GWPE and the 200 hPa eastward wind anomalies at $\sim -20 - 0^{\circ}$ longitudinal lag (see supporting information Figure S2). This demonstrates that the modulation of stratospheric GWPE at 26 km is strongly correlated with the dynamic variability of the MJO as measured by the 200 hPa zonal wind anomalies.

We propose that this correlation is a result of the filtering of upward propagating gravity waves by the MJO wind anomalies, which impose an MJO modulation on the GWPE. To investigate this mechanism, we will now consider the range of absolute winds (i.e., background plus anomaly) encountered by such waves at different points in the MJO phase and consider the filtering effects on the waves of these winds.

First, we will illustrate the concept of the proposed mechanism by considering the winds encountered by upward propagating gravity waves at two different locations during MJO phase 3 and phase 6. The locations are (170° E, 10°S) and (60°W, 10°S). They are arbitrarily chosen to represent regions of increased and reduced

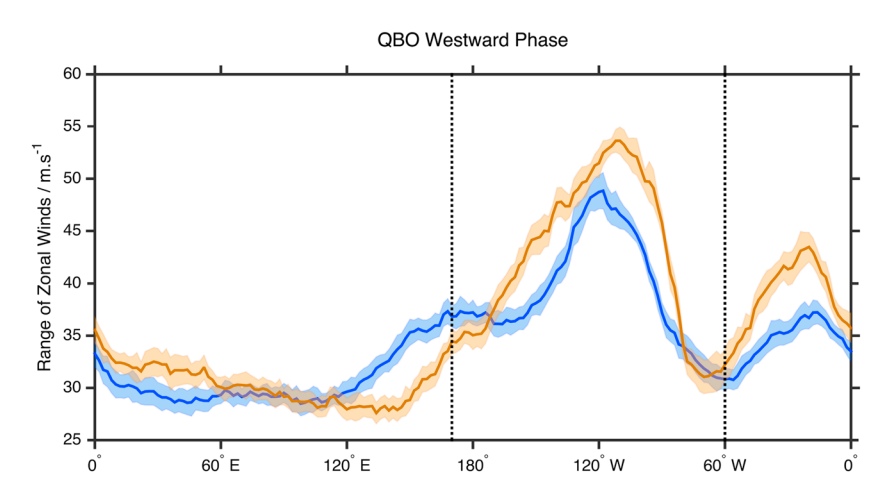


Figure 5. Bootstrapped distribution (1000 samples) of nonbandpassed ECMWF zonal wind absolute range between 10 and 26 km (i.e., the height range considered in Figure 4) against longitude for the QBO westward phase at 10°S. The shading shows the 95% confidence interval on the mean (thick line) of the bootstrapped distribution for MJO phase 3 (blue) and phase 6 (orange). In both panels the vertical black dotted lines highlight the locations indicated by crosses in Figure 3.

GWPE. Each location is indicated by black crosses in Figure 3. The composite mean unfiltered ECMWF zonal wind speed from 5 to 30 km at these two locations in MJO phases 3 and 6 is presented in Figure 4. In each plot the range of winds encountered between 10 km and 26 km is bound by the dotted vertical lines and filled by the blue shading. The thick horizontal black bars indicate the total range of winds encountered between 10 and 26 km in each case.

Figure 4 (left column) shows the range of winds for (170°E, 10°S), where reduced GWPE and stronger eastward wind anomalies occur in phase 3 and vice versa in phase 6. Examination of the figure shows that a wider range of winds is encountered by upward propagating waves in phase 3 $(-14.1 \text{ m s}^{-1} \text{ to } 6.19 \text{ m s}^{-1})$ compared to phase 6 (-14.0 m s⁻¹ to 1.14 m s⁻¹). This wider range results from the winds in phase 3 being more eastward in the upper troposphere and peaking around 13 km, which is approximately 200 hPa. In contrast, a smaller range of eastward winds are encountered in phase 6, when GWPE is greater.

Figure 4 (right column) shows the range of winds for (60°W, 10°S). Here greater GWPE and stronger westward wind anomalies occur in phase 3 and vice versa in phase 6. A wider range of winds is observed in phase 6 $(-15.8 \text{ m s}^{-1} \text{ to } 0.25 \text{ m s}^{-1})$ compared to phase 3 $(-15.7 \text{ m s}^{-1} \text{ to } -2.63 \text{ m s}^{-1})$. This increase in range is due to a shift eastward in the upper tropospheric winds in phase 6, where reduced GWPE is observed.

The spectrum of gravity wave phase speeds is known to be centered at low values [e.g., Fritts and Alexander, 2003]. The winds in Figure 4 will thus progressively filter out such gravity waves as they propagate to heights where their zonal phase speeds equal the local zonal wind and where they are then absorbed at a critical level. As the local wind includes the MJO anomaly, this process can thus imprint a signature of the MJO anomaly on the field of upward propagating waves. The variation of winds and GWPE at the points considered in Figure 4 is thus consistent with this proposed filtering. However, the data presented in the analysis of Figure 4 are only for the two arbitrarily selected locations. We will therefore now generalize this analysis to consider the winds encountered by gravity waves at all longitudes. Further, it is known that the stratospheric GWPE is modulated by the phase of the QBO [e.g., Alexander et al., 2008], so we will also sort the data by QBO phase.

In this second analysis, we examine the range of zonal winds encountered between 10 and 26 km by upward propagating waves at all longitudes for each QBO phase. We use bootstrapping [e.g., Efron, 1979; Wright et al., 2012] to calculate, as a function of longitude, the distribution of zonal wind ranges and their various percentiles, for increments of 2° longitude. This bootstrapping provides a measure of the uncertainty of the winds. The bootstrapping is done by randomly sampling days from the time series 1000 times for days sorted by both QBO phase and MJO phase.

To illustrate the results of this analysis, we will consider the case where the QBO is westward and the MJO is in phase 3 and phase 6. We present in Figure 5 the magnitude of the range of winds encountered between 10 km and 26 km range for MJO phase 3 (solid blue line) and MJO phase 6 (solid orange line). Also indicated by



shading is the 95% confidence interval from the bootstrapping. Finally, the two vertical dashed lines indicate the longitudes of the two arbitrary locations considered above.

From Figure 5 it can be seen that the zonal wind range was generally *larger* in phase 3 than phase 6 at longitudes between approximately 120°E to 170°W (i.e., where the GWPE was smaller during phase 3 than phase 6—see Figure 3). Conversely, the zonal wind range was smaller in phase 3 than phase 6 at most other longitudes (i.e., where the GWPE was larger during phase 3 than phase 6—see Figure 3). An examination of the absolute values of the winds reveals that the variability occurs largely in the eastward component of the winds. Similar results are found comparing the winds and GWPE for the other MJO phases. Similar results are also observed for the QBO eastward phase but are less clearly defined (see supporting information Figure S3). The confidence intervals shown in the figure indicate that this result is statistically significant to at least 95% confidence level. The MJO period modulation of GWPE, as presented in Figure 3, is observed more clearly during the westward phase of the QBO compared to the eastward phase (see supporting information Figures S4 and S5, respectively). Thus, our results provide clearer evidence of MJO modulation of GWPE by the MJO zonal wind anomalies during the QBO westward phase and a reduced effect during the QBO eastward phase. This is most likely a consequence of the larger amplitude zonal winds in the westward phase [e.g., Baldwin, 2001]. Collectively, our results show that at a given latitude, the larger range of wind speeds encountered between 10 km and 26 km as a result of the MJO is associated with reduced GWPE at 26 km and vice versa.

4. Discussion

There are two principal methods whereby the MJO might modulate the field of stratospheric gravity waves. First, the modulation of convection by the MJO might modulate the excitation of gravity waves. Second, the MJO wind anomalies in the troposphere might modulate the wave propagation environment through critical-level filtering. Both of these mechanisms might thus modulate the field of gravity waves that reach the stratosphere.

There exist very few studies investigating the influence of the MJO on stratospheric gravity waves. However, Horinouchi [2008] suggested that the reduced convection during the inactive phase of the MJO would nevertheless generate larger fluxes of stratospheric gravity wave energy and momentum than the active phase because of the longer vertical wavelengths generated being better able to propagate vertically. Our results indicate a strong correlation between GWPE and the anomalous zonal winds of the MJO, suggesting that wave critical-level filtering plays an important role. However, these results are not necessarily contradictory because the waves considered by Horinouchi [2008] are of significantly shorter horizontal wavelength and higher frequency than those accessible by COSMIC RO measurements.

Here we have proposed that the MJO wind anomalies cause the GWPE anomalies of Figure 3. However, we should note that this mechanism will be sensitive to the horizontal phase speed distribution of the gravity waves. In particular, the mechanism assumes that a significant fraction of the waves have eastward phase speeds such that the waves will be filtered out by the eastward wind anomalies of the MJO. Our COSMIC RO measurements provide no information on wave horizontal phase speeds, and our assumption cannot therefore be tested with this data set. Nevertheless, our results suggest that the MJO plays a significant role in modulating the stratospheric gravity wave field.

5. Conclusion

The MJO is the dominant driver of intraseasonal variability in the tropical troposphere. Our observations show a strong correlation between stratospheric GWPE and the anomalous tropospheric zonal winds of the MJO when the observations are sorted by MJO phase. We have proposed that this correlation is a result of a filtering of the gravity wave field by these winds which removes primarily eastward propagating waves during the MJO eastward wind anomalies. These results highlight the importance of tropospheric processes in controlling the stratospheric gravity wave field.

References

Alexander, M. J., et al. (2010), Recent developments in gravity-wave effects in climate models and the global distribution of gravity-wave momentum flux from observations and models, Q. J. R. Meteorol. Soc., 136(650), 1103-1124, doi:10.1002/qj.637. Alexander, S. P., T. Tsuda, Y. Kawatani, and M. Takahashi (2008), Global distribution of atmospheric waves in the equatorial upper troposphere and lower stratosphere: COSMIC observations of wave mean flow interactions, J. Geophys. Res., 113, D24115, doi:10.1029/2008JD010039.

Acknowledgments

A.C. Moss was funded by a PhD studentship from the U.K. Natural **Environment Research Council** (NERC), and C.J. Wright and N.J. Mitchell by NERC grant NE/K015117/1. COSMIC Radio Occultation Data can be obtained from the COSMIC Data Analysis and Archive Centre, and ECMWF reanalyses data can be obtained from the British Atmospheric Data Centre. We are grateful to Neil Hindley for helpful suggestions and discussions. We would also like to thank an anonymous reviewer for important statistical suggestions. which have greatly enhanced the final version of this manuscript.

- Alexander, S. P., A. R. Klekociuk, and T. Tsuda (2009), Gravity wave and orographic wave activity observed around the Antarctic and Arctic stratospheric vortices by the COSMIC GPS-RO satellite constellation, J. Geophys. Res., 114, D17103, doi:10.1029/2009JD011851.
- Baldwin, M. P. (2001), The quasi-biennial oscillation, Rev. Geophys., 39(2), 179–229, doi:10.1029/1999RG000073.
- CLIVAR Madden-Julian Oscillation Working Group (2009), MJO simulation diagnostics, J. Clim., 22, 3006–3030, doi:10.1175/2008JCLI2731.1.
- Davis, R. N., Y.-W. Chen, S. Miyahara, and N. J. Mitchell (2012), The climatology, propagation and excitation of ultra-fast Kelvin waves as observed by meteor radar, Aura MLS, TRMM and in the Kyushu-GCM, Atmos. Chem. Phys., 12, 1865–1879, doi:10.5194/acp-12-1865-2012.
- Duchon, C. E. (1979), Lanczos filtering in one and two dimensions, *J. Appl. Meteor.*, 18, 1016–1022, doi:10.1175/1520-0450(1979)018<1016%3ALFIOAT>2.0.CO%3B2.
- Eckermann, S. D., D.-K. Rajopadhyaya, and R. A. Vincent (1997), Intraseasonal wind variability in the equatorial mesosphere and lower thermosphere: Long-term observations from the central Pacific, *J. Atmos. Sol. Terr. Phys.*, *59*(6), 603–627, doi:10.1016/S1364-6826(96)00143-5.
- Efron, B. (1979), Bootstrap methods: Another look at the jackknife, Ann. Stat., 7(1), 1-26, doi:10.1214/aos/1176344552.
- Faber, A., P. Llamedo, T. Schmidt, A. de la Torre, and J. Wickert (2013), On the determination of gravity wave momentum flux from GPS radio occultation data, *Atmos. Meas. Tech.*, 6, 3169–3180, doi:10.5194/amt-6-3169-2013.
- Fritts, D. C., and M. J. Alexander (2003), Gravity wave dynamics and effects in the middle atmosphere, *Rev. Geophys.*, 41(1), 1003, doi:10.1029/2001RG000106.
- Hamilton, K., R. A. Vincent, and P. T. May (2004), Darwin Area Wave Experiment (DAWEX) field campaign to study gravity wave generation and propagation, *J. Geophys. Res.*, 109, D20S01, doi:10.1029/2003JD004393.
- Hindley, N. P., C. J. Wright, N. D. Smith, and N. J. Mitchell (2015), The southern stratospheric gravity wave hot spot: Individual waves and their momentum fluxes measured by COSMIC GPS-RO, Atmos. Chem. Phys., 15, 7797–7818, doi:10.5194/acp-15-7797-2015.
- Horinouchi, T. (2008), A numerical study of upward-propagating gravity waves in two different MJO phases, *Geophys. Res. Lett.*, 35, L17802, doi:10.1029/2008GL034992.
- Isoda, F., T. Tsuda, T. Nakumura, R. A. Vincent, I. M. Reid, E. S. A. Achmad, and A. Nuryanto (2004), Intraseasonal oscillations of the zonal wind near the mesopause observed with medium-frequency and meteor radars in the tropics, *J. Geophys. Res., 109*, D21108, doi:10.1029/2003JD003378.
- Karoly, D. J., G. L. Roff, and M. J. Reeder (1996), Gravity wave activity associated with tropical convection detected in TOGA COARE sounding data, *Geophys. Res. Lett.*, 23(3), 261 264, doi:10.1029/96GL00023.
- Khouider, B., A. St-Cyr, A. J. Majda, and J. Tribbia (2011), The MJO and convectively coupled waves in a coarse-resolution GCM with a simple multicloud parameterization, *J. Atmos. Sci.*, 68(2), 240–264, doi:10.1175/2010JAS3443.1.
- Kursinski, E. R., G. A. Hajj, J. T. Schofield, R. P. Linfield, and K. R. Hardy (1997), Observing Earth's atmosphere with radio occultation measurements using the Global Positioning System, *J. Geophys. Res.*, 102, 23,429–23,465, doi:10.1029/97JD01569.
- Liou, Y., A. G. Pavelyev, S. Liu, A. A. Pavelyev, N. Yen, C.-Y. Huang, and C. Fong (2007), FORMOSAT-3/COSMIC GPS radio occultation mission: Preliminary results, *IEEE Trans. Geosci. Remote Sens.*, 45, 3813–3826, doi:10.1109/TGRS.2007.903365.
- Madden, R. A., and P. R. Julian (1972), Description of global-scale circulation cells in the tropics with a 40–50 day period, *J. Atmos. Sci.*, 29(6), 1109–1123, doi:10.1175/1520-0469%281972%29029<1109%3ADOGSCC>2.0.CO%3B2.
- Marquardt, C., and S. Healy (2005), Measurement noise and stratospheric gravity wave characteristics obtained from GPS occultation data, J. Meteorol. Soc. Jpn., 83(3), 417–428, doi:10.2151/jmsj.83.417.
- Matthews, A. J. (2000), Propagation mechanisms for the Madden-Julian Oscillation, Q. J. R. Meteorol. Soc., 126, 2637–2652, doi:10.1002/qj.49712656902.
- McDonald, A. J. (2012), Gravity wave occurrence statistics derived from paired COSMIC/FORMOSAT3 observations, J. Geophys. Res., 117, D15106. doi:10.1029/2011/JD016715.
- Morita, J., Y. N. Takayabu, S. Shige, and Y. Kodama (2006), Analysis of rainfall characteristics of the Madden-Julian Oscillation using TRMM satellite data, *Dyn. Atmos. Oceans*, 42(1–4), 107–126, doi:10.1016/j.dynatmoce.2006.02.002.
- Rao, R. K., et al. (2009), Longitudinal variability in intraseasonal oscillation in the tropical mesosphere and lower thermosphere region, J. Geophys. Res., 114, D19110, doi:10.1029/2009JD011811.
- Salby, M. L., R. R. Garcia, and H. H. Hendon (1994), Planetary-scale circulations in the presence of climatological and wave-induced heating, J. Atmos. Sci., 51(16), 2344–2367, doi:10.1175/1520-0469(1994)051<2344%3APSCITP>2.0.CO%3B2.
- Sperber, K. R. (2003), Propagation and the vertical structure of the Madden-Julian Oscillation, *Mon. Weather Rev.*, 131, 3018–3037, doi:10.1175/1520-0493(2003)131<3018%3APATVSO>2.0.CO%3B2.
- Stockwell, R. G., L. Manshinha, and R. P. Lowe (1996), Localization of the complex spectrum: The Stransform, *IEEE Trans. Signal Process.*, 44(4), 998–1001, doi:10.1109/78.492555.
- Tsuda, T., M. Nishida, C. Rocken, and R. H. Ware (2000), A global morphology of gravity wave activity in the stratosphere revealed by the GPS occultation data (GPS/MET), J. Geophys. Res., 105(D6), 7257–7273, doi:10.1029/1999JD901005.
- Tsuda, T., X. Lin, H. Hayashi, and Noersomadi (2011), Analysis of vertical wave number spectrum of atmospheric gravity waves in the stratosphere using COSMIC GPS radio occultation data, Atmos. Meas. Tech., 4, 1627–1636, doi:10.5194/amt-4-1627-2011.
- Wang, L., and M. J. Alexander (2010), Global estimates of gravity wave parameters from GPS radio occultation temperature data, J. Geophys. Res., 115, D21122, doi:10.1029/2010JD013860.
- Wheeler, M. C., and H. H. Hendon (2004), An all-season real-time multivariate MJO index: Development of an index for monitoring and prediction, *Mon. Weather Rev.*, 132(8), 1917–1932, doi:10.1175/1520-0493(2004)132<1917%3AAARMMI>2.0.CO%3B2.
- Wheeler, M. C., H. H. Hendon, S. Cleland, H. Meinke, and A. Donald (2009), Impacts of the Madden-Julian Oscillation on Australian rainfall and circulation, *J. Clim.*, 22(6), 1482 1498, doi:10.1175/2008JCLI2595.1.
- Wright, C. J., and J. C. Gille (2011), HIRDLS observations of gravity wave momentum fluxes over the monsoon regions, *J. Geophys. Res.*, 116, D12103, doi:10.1029/2011JD015725.
- Wright, C. J., M. B. Rivas, and J. C. Gille (2011), Intercomparisons of HIRDLS, COSMIC and SABER for the detection of stratospheric gravity waves, *Atmos. Meas. Tech.*, 4, 1581–1591, doi:10.5194/amt-4-1581-2011.
- Wright, C. J., R. B. Scott, B. K. Arbic, and D. F. Furnival (2012), Bottom dissipation of subinertial currents at the Atlantic zonal boundaries, J. Geophys. Res., 117, C03049, doi:10.1029/2011JC007702.
- Wright, C. J., N. P. Hindley, A. C. Moss, and N. J. Mitchell (2015), Multi-instrument gravity-wave measurements over Tierra del Fuego and the Drake Passage—Part 1: Potential energies and vertical wavelengths from AIRS, COSMIC, HIRDLS, MLS-Aura, SAAMER, SABER and radiosondes, *Atmos. Meas. Tech. Discuss.*, 8(7), 6797–6876, doi:10.5194/amtd-8-6797-2015.
- Zhang, C. (2005), Madden-Julian Oscillation, Rev. Geophys., 43, RG2003, doi:10.1029/2004RG000158.